Applied Catalysis B: Environmental 165 (2015) 661–667

Contents lists available at ScienceDirect

Applied Catalysis B: Environmental

journal homepage: www.elsevier.com/locate/apcatb

Green Suzuki–Miyaura coupling reaction catalyzed by palladium nanoparticles supported on graphitic carbon nitride

Jingwen Sun[a,b], Yongsheng Fu[a,*], Guangyu He[b], Xiaoqiang Sun[b,*], Xin Wang[a,*]

[a] Key Laboratory of Soft Chemistry and Functional Materials, Nanjing University of Science and Technology, Ministry of Education, Nanjing 210094, China
[b] Key Laboratory of Fine Petrochemical Engineering, Changzhou University, Changzhou 213164, China

ARTICLE INFO

Article history:
Received 10 September 2014
Received in revised form 12 October 2014
Accepted 27 October 2014
Available online 3 November 2014

Keywords:
Palladium nanoparticles
Graphitic carbon nitride
Green Suzuki–Miyaura reaction
Mild conditions

ABSTRACT

The synthesis of biphenyls under mild conditions is really a challenge to green chemistry. Here we report a facile photodeposition strategy to fabricate a Pd/g-C_3N_4 nanocomposite and demonstrate its application as a green catalyst for Suzuki–Miyaura coupling reactions. The Pd nanoparticles with an average size of 2.73 nm are uniformly dispersed on the g-C_3N_4 surface. The Pd/g-C_3N_4 nanocomposite shows superior catalytic activity in Suzuki–Miyaura coupling reactions at room temperature without any phase transfer agents, toxic solvents and inert atmosphere, especially, allowing a complete conversion (100%) of bromobenzene and a high yield of 97% for biphenyl. The high catalytic performance of Pd/g-C_3N_4 nanocomposite in Suzuki–Miyaura coupling reactions can be attributed to the specific characteristics of the unique nanostructure of Pd/g-C_3N_4 and the concerted effects of g-C_3N_4 and ultrafine Pd particles.

1. Introduction

The development of approaches for forming C—C bonds plays an important role in organic synthesis. The Pd-catalysed Suzuki–Miyaura coupling reaction has become a central tool for the construction of C—C bonds, widely used to synthesize natural products, non-natural products, and other bioactive compounds, as well as some advanced materials [1–4]. Traditionally, the C—C coupling reactions are carried out in organic solvents such as tetrahydrofuran and diethyl ether in the presence of Pd(II) or Pd(0) complexes having organic ligands at higher temperatures [5–7]. However, there are some glaring disadvantages in this case. First of all, the employed organic solvents may cause serious environmental problems due to their toxicity and the reactions carried out at higher temperatures definitely consume more energy, generate more oxides of nitrogen and other harmful gases. Secondly, the most common catalytic system used for Suzuki–Miyaura coupling reaction is the homogeneous palladium complexes with expensive and air-sensitive phosphine ligands in presence of base, leading to high production cost [8]. Furthermore, there is a common problem in homogeneous catalysts, the difficulty of catalyst separation and reuse, which also restricts their industrial application [9–11].

Supported metal nanoparticles (NPs) play a pivotal role in a wide range of applications, especially in the area of catalysis. Among the various metal NPs, platinum group metals (PGMs) are used most extensively as the catalysts for a great many industrial applications in hydrogenation [12], hydroformylation [13], carbonylation [14,15], and so on. Over the past few decades, palladium NPs have also been applied as the most efficient catalyst to C—C coupling reactions like Suzuki–Miyaura coupling reactions on account of the economic benefits. Nevertheless, there are a number of challenges and obstacles such as easy aggregation of the nanoparticles and low utilization efficiency of Pd to limit the practical application. An alternative way to solve this problem is effectively controlling and stabilizing the size and morphology of Pd nanostructures by highly dispersing Pd nanoparticles on a high surface area support, such as metal oxides [16], organic-inorganic composites [17,18], inorganic porous materials [19], polymers [20] and carbon materials [21–23].

Recently, polymeric mesoporous graphitic carbon nitrides (g-C_3N_4) has been widely studied in the field of photocatalysis due to its high thermal stability against high temperatures and chemical stability against acid, base and organic solvents, and semiconducting properties [24–28]. Unlike the traditional carbon materials, g-C_3N_4 possesses a stacked two-dimensional structure and can be regarded as a promising source for the mass-production of free-standing nitrogen-rich carbon materials, which is propitious to disperse and stabilize the Pd nanoparticles [29,30].

It is therefore of great interest to design and fabricate a multifuctional g-C_3N_4-based composite on the basis of sufficient utilization its abundant basic sites. If that can be accomplished, then it may be

* Corresponding authors.
E-mail addresses: fuyongsheng@mail.njust.edu.cn (Y. Fu), sun@cczu.edu.cn (X. Sun), wangx@njust.edu.cn (X. Wang).

http://dx.doi.org/10.1016/j.apcatb.2014.10.072
0926-3373/

possible to obtain an advanced catalyst for Suzuki–Miyaura coupling reactions at lower temperatures. Herein, we demonstrate a facile one-step photodeposition method to fabricate Pd/g-C_3N_4 nanocomposite. The Pd NPs with an average size of 2.73 nm were uniformly dispersed on the g-C_3N_4 surface. Surprisingly, the as-prepared Pd/g-C_3N_4 nanocomposite exhibited superior catalytic activity in Suzuki–Miyaura coupling reactions at room temperature without any phase transfer agents, toxic solvents and inert atmosphere, achieving a green and high-efficient chemical synthesis.

2. Experimental

2.1. Synthesis of Pd/g-C_3N_4 nanocatalyst

The supporting mesoporous g-C_3N_4 was synthesized by directly heating cyanamide (CN—NH_2) in a ceramic combustion boat, which was heated in a furnace from room temperature to 550 °C at a rate of 2.3 °C min^{-1} and calcined at 550 °C for 4 h under flowing N_2. The as-obtained yellow powder of g-C_3N_4 was ground in a mortar. A typical experiment for the synthesis of Pd/g-C_3N_4 nanocatalyst with 10 wt% Pd is as follows: g-C_3N_4 (20 mg) was dispersed in isopropyl alcohol (200 mL) with sonication in a low power sonic bath for 30 min. As-obtained g-C_3N_4 dispersion was stirred, while 20 μL of $Pd(NO_3)_2$ diluted in HNO_3 solution (1 M) was added under continuous stirring for 2 h at room temperature, accompanied by the chelate adsorption of Pd^{2+} on g-C_3N_4. The reaction mixture was irradiated with a high pressure Hg lamp (500 W) for 30 min at room temperature and the color of the mixture changed gradually from light yellow to grayish brown. The product, denoted as $Pd_{0.10}$/g-C_3N_4, was centrifuged, washed with deionized water. Finally the water of the product was removed through freeze drying. For comparison, $Pd_{0.05}$/g-C_3N_4 and $Pd_{0.20}$/g-C_3N_4 composites were also prepared under the same experimental conditions.

2.2. Characterization

Transmission electron microscopy (TEM) images were taken using a JEOL JEM-2100 microscope operating at 200 kV, by depositing a drop of sample dispersion onto 300 mesh Cu grids 45 coated with a carbon layer. Inductively coupled plasma atomic emission spectrometry (ICP-AES, Shimadzu ICP-7510) was employed to determine the exact amounts of Pd. Brunauer–Emmett–Teller (BET) surface area was obtained by nitrogen sorption experiments conducting at 77 K using a Micromeritics TriStar II 3020 automated gas adsorption analyzer. Powder X-ray diffraction (XRD) analyses were performed on a Bruker D8 Advanced diffractometer with Cu Kα radiation and the scanning angle ranged from 5° to 70° of 2θ. Fourier transform infrared (FTIR) spectra were recorded on a Bruker VECTOR 22 spectrometer using the KBr pellet technique. X-ray 50 photoelectron spectroscopy (XPS) measurements were carried out on a RBD upgraded PHI-5000C ESCA system (Perkin Elmer) with Mg Kα radiation ($h\nu$ = 1253.6 eV).

2.3. Suzuki–Miyaura coupling reaction

In a typical reaction, phenylboronic acid (0.24 mmol, 1.20 equiv), KOH (0.60 mmol, 3 equiv) and $Pd_{0.10}$/g-C_3N_4 (2 mg) were codissolved or dispersed in a mixture of 4 mL H_2O:EtOH (1:1) and sonicated for 5 min to obtain a uniform dispersion. Then aryl halides (0.20 mmol, 1 equiv) was added into the dispersion under magnetic stirring at room temperature for 1 h. When the reaction completed, the resulting solution was extracted with ethyl acetate. The organic layers were combined, dried over anhydrous Na_2SO_4, and filtered. The solvent in the filtrate was then removed in vacuo to give a solid. Reagent conversions and product yields were determined by HPLC analysis (SHIMADZU LC-20A) on the basis of aryl halides. After the reaction, catalysts were easily collected by centrifugation, washed with NaOH aqueous solution for several times to remove the adsorbed bromobenzene, and then vacuum freeze-dried. It is worthy to note that the recycle catalyst can be reused five times in succession without noticeable loss of its activity. To further investigate the factors that may influence the activity, a series of Suzuki coupling reactions has been conducted with different reagents under various conditions.

3. Results and discussion

3.1. Structure and morphology of Pd/g-C_3N_4 nanocomposite catalyst

As shown in Fig. 1a, g-C_3N_4 shows a typical platelet-like morphology with several layers. With lower palladium contents ($Pd_{0.05}$/g-C_3N_4 and $Pd_{0.10}$/g-C_3N_4), smaller Pd NPs were uniformly dispersed on the surface of g-C_3N_4 (Fig. 1b and c). The high-resolution transmission electron microscopy (HRTEM) pattern further confirmed the crystalline nature of Pd nanoparticles and lattice spacing of 0.226 nm, corresponding to the interplanar spacing of Pd (1 1 1) [31]. Based on the particle size distribution histograms obtained by measuring the sizes of 200 randomly chosen particles (Fig. 1d), the average particle size was estimated to be about 2.73 nm with a narrow size distribution. As shown in Fig. 1e, at a high loading amount (~20%), the Pd NPs tend to aggregate, which may be a fatal factor leading to a decrease in catalytic activity [32]. The exact amounts of Pd in Pd/g-C_3N_4 and Pd/AC were detected via ICP-AES and contents of Pd in $Pd_{0.05}$/g-C_3N_4, $Pd_{0.10}$/g-C_3N_4, $Pd_{0.20}$/g-C_3N_4, and commercial $Pd_{0.10}$/AC were measured at 4.4 wt%, 8.8 wt%, 17.6 wt% and 9.3 wt%, respectively.

The pore size distribution (Fig. 1f) was obtained by measuring their nitrogen adsorption–desorption isotherm (the inset of Fig. 1f). The specific surface area of the catalyst was determined to be 37.13 m^2 g^{-1} using the Brunauer–Emmett–Teller (nitrogen, 77 K) method and the BJH desorption average pore diameter was 3.40 nm with very narrow pore size distribution.

Fig. 2a shows the X-ray diffraction (XRD) patterns of g-C_3N_4 and the as-prepared $Pd_{0.10}$/g-C_3N_4 nanocomposite, respectively. The most intense peak at 27.40° of g-C_3N_4 may be assigned to the (0 0 2) plane of graphitic stacking g-C_3N_4, and the calculated interplanar distance of aromatic units (d = 0.33 nm) is close to that of the crystalline g-C_3N_4 (d = 0.34 nm) [23,33–35]. The other characteristic peak at 13.00° of g-C_3N_4, corresponding to interplanar distance of 0.68 nm, can be indexed as (1 0 0), which belongs to an in-plane structural packing motif between nitride pores [36]. After the loading of Pd NPs, the peak of $Pd_{0.10}$/g-C_3N_4 composite at 27.40° was significantly reduced and the peak at 13.00° was broadened substantially due to the disturbance of the graphitic structure after the loading [37]. While, the peaks at 40.02°, 46.59° and 68.08° can be indexed as the (1 1 1), (200) and (220) planes of the face-centered cubic structure of Pd (JCPDS 46-1043), respectively [23,26].

The FTIR spectra of samples are shown in Fig. 2b. For g-C_3N_4, the broad bands in the 3500–2800 cm^{-1} region can be assigned NH stretching vibration modes [34], while the strong bands between 1000 and 1650 cm^{-1}, deriving from the typical stretching vibration modes of C=N and C—N heterocycles [38], were also detected as the characteristic peaks of s-triazine derivatives [39]. Thus, the trigonal C—N(—C)—C (full condensation) and the bridging C—NH—C units (partial condensation) were both formed in the polymer during the thermal conversion [40]. Additionally, the significant band at 810 cm^{-1} can be assigned to the characteristic ring-sextant out-of-plane bending vibration of triazine units [38,40]. After the introduction of Pd NPs, no noticeable change in the main characteristic bands of g-C_3N_4 can be observed, indicating that there is

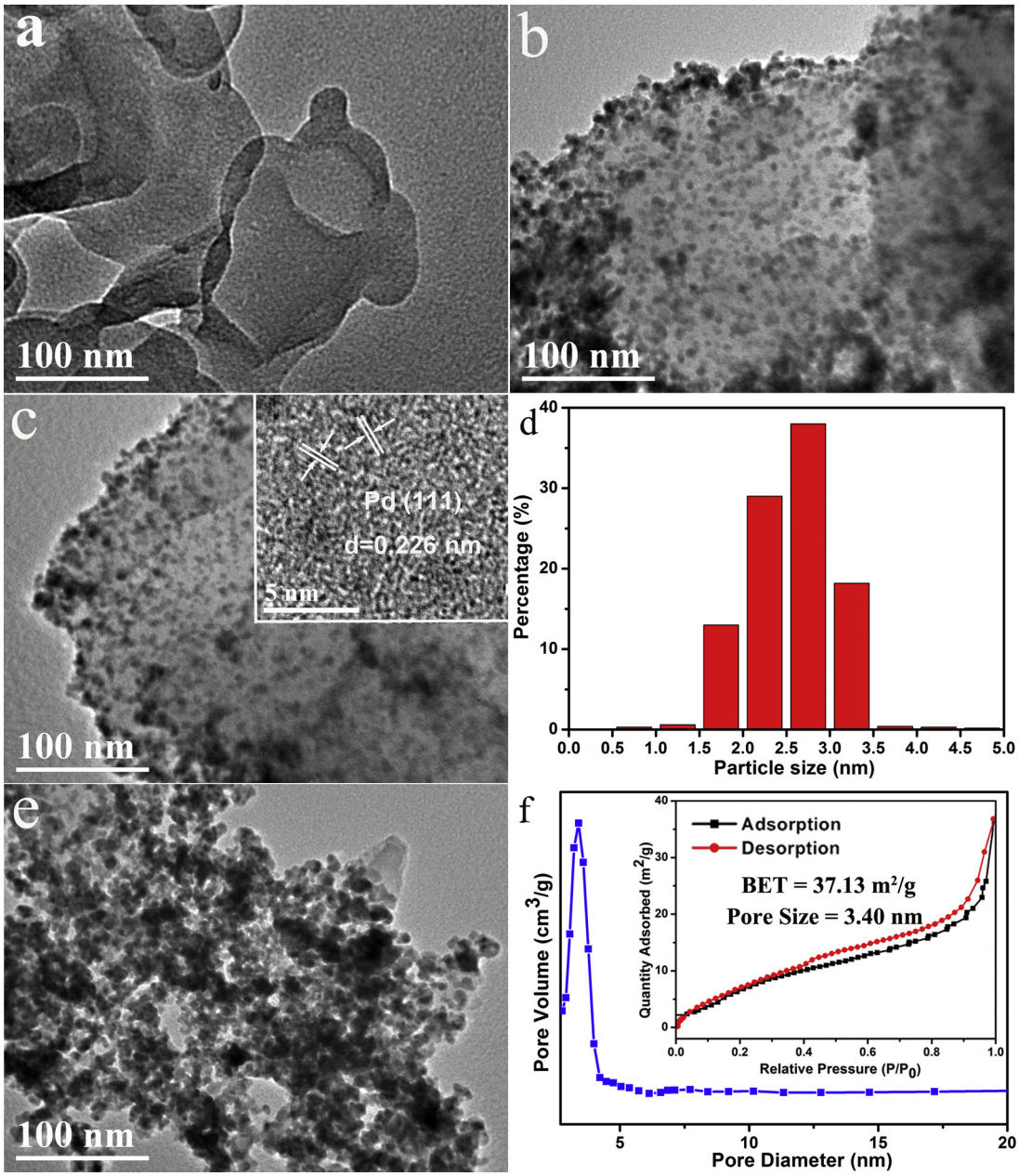

Fig. 1. TEM images of (a) pure g-C_3N_4, (b) $Pd_{0.05}$/g-C_3N_4. (c) TEM image and HRTEM image (inset) of $Pd_{0.10}$/g-C_3N_4. (d) The size distribution of $Pd_{0.10}$/g-C_3N_4 nanoparticles. (e) TEM image of $Pd_{0.20}$/g-C_3N_4 nanocomposite. (f) Pore size distribution curves and the corresponding nitrogen adsorption–desorption isotherms (inset) for $Pd_{0.10}$/g-C_3N_4.

non-covalently coupled interaction between g-C_3N_4 and Pd NPs in the composite.

X-ray photoelectron spectroscopy (XPS) was used to determine the surface elemental composition with oxidation state information for the $Pd_{0.10}$/g-C_3N_4 nanocomposite. The XPS survey spectrum of $Pd_{0.10}$/g-C_3N_4 nanocomposite is shown in Fig. 3a, revealing the co-existence of C, N, O and Pd in the sample. As shown in Fig. 3b, the C 1s spectrum of $Pd_{0.10}$/g-C_3N_4 can be deconvoluted into two peak components with binding energies at 284.60 and 288.10 eV, corresponding to the C—C sp^2 N=C—N species, respectively. While the N 1s spectrum can be resolved into three peaks centered at the binding energies of 398.60, 400.00 and 401.10 eV, corresponding to the C=N—C, N—$(C)_3$ and C—N—C species, respectively (Fig. 3c). These assignments are in good agreement with the previous reports of graphitic carbon nitride powders [33,38]. The XPS spectrum of Pd 3d in the nanocomposite consists of two doublets (Fig. 3d), the intensive doublet (335.6 and 340.8 eV) may be assigned to metallic Pd and the other doublet (337.8 and 343.2 eV) belongs to the +2 oxidation state of Pd [32]. Based on the peak areas, Pd^0 was estimated to be 87.5% in whole Pd atoms. The existence of Pd^{2+} in the catalyst contributed to the fact that the reduction of Pd^{2+} had not been entirely completed during the preparation or the naked metal Pd atoms would be easily oxidized to the form of Pd^{2+} at ambient conditions.

3.2. Suzuki–Miyaura coupling reaction

The Suzuki–Miyaura coupling reaction of bromobenzene with phenylboronic acid (Scheme 1) was chosen as a model reaction to evaluate the catalytic activities of Pd/g-C_3N_4 (5, 10 and 20 wt%) nanocomposites and commercial Pd/AC (10%). This reaction is usually carried out with an aqueous inorganic base and a phase transfer catalyst in organic solvents at relatively higher temperatures, generally under an inert atmosphere to avoid the oxidation of the

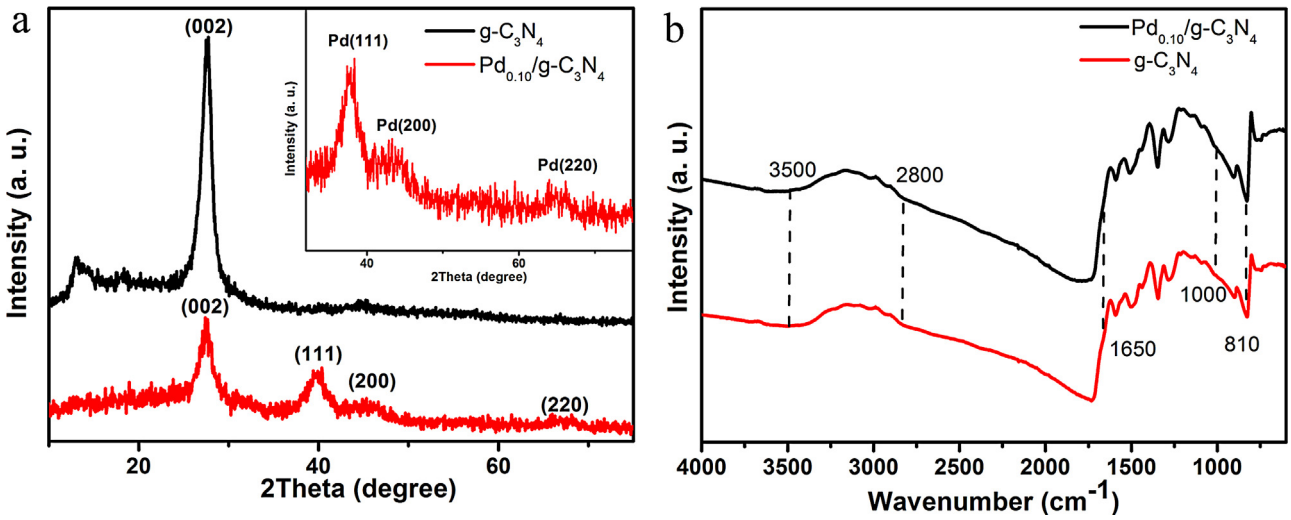

Fig. 2. XRD patterns (a) and FTIR absorbance (b) spectra of pure g-C_3N_4 and $Pd_{0.10}$/g-C_3N_4, respectively.

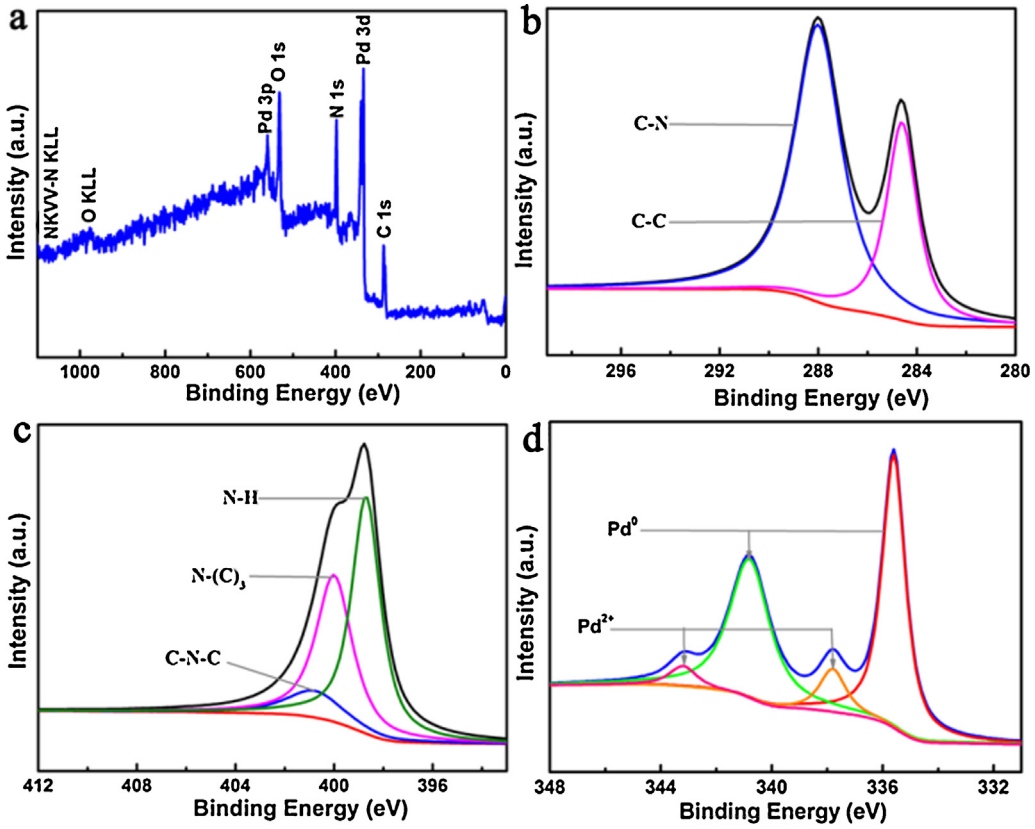

Fig. 3. (a) XPS survey spectrum of $Pd_{0.10}$/g-C_3N_4 nanocomposite, (b) C 1s, (c) N 1s and (d) Pd 3d core-level XPS spectra, respectively.

Pd-based catalysts. In this study, however, the Suzuki reaction can be conducted in aqueous-ethanol (1:1) with KOH as base at room temperature without any phase transfer agents, toxic solvents and inert atmosphere.

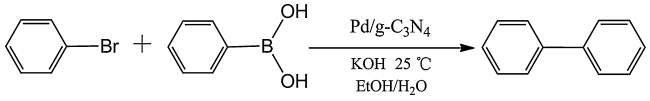

Scheme 1. Suzuki–Miyaura coupling reaction.

Fig. 4a shows the conversion of bromobenzene over its initial concentration plots at intervals for the Suzuki–Miyaura coupling reaction in the presence of various catalysts. It should be noted that the catalytic activities of the as-prepared Pd/g-C_3N_4 increases first and then decreases as palladium content increases. Among them, $Pd_{0.10}$/g-C_3N_4 catalyst exhibited the best catalytic performance, and the conversion of bromobenzene reached to 100% only within 40 min, much higher than the commercial Pd/AC with the same Pd content. This result was also supported by TEM studies. As shown in Fig. 1e, the aggregation of Pd NPs really occurred for $Pd_{0.20}$/g-C_3N_4. High Pd loading may result not only in high costs for preparation of catalysts, but also in the increase in particle size and

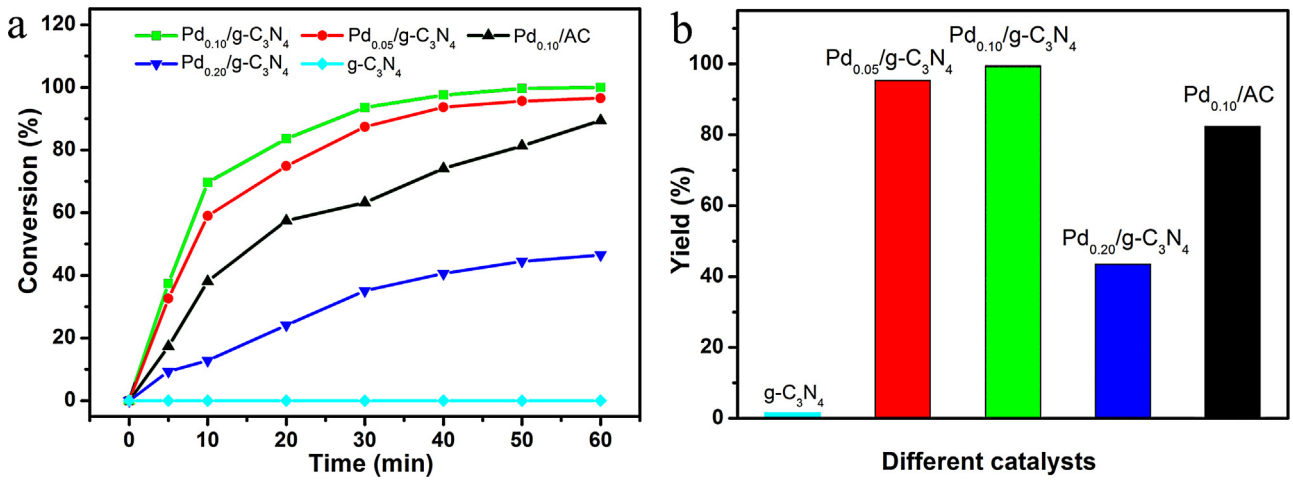

Fig. 4. (a) Conversion of bromobenzene over its initial concentration plots at intervals with various catalysts, (b) yields of biphenyl catalyzed by different catalysts.

aggregation, leading to lower catalytic activities [32]. Besides, Fig. 4b gives the yields of biphenyl catalyzed by various catalysts with the same time, which attests to much higher yield by $Pd_{0.10}/g\text{-}C_3N_4$.

In order to elucidate the reaction kinetic process, pseudo-second-order kinetic model has been employed to fit the experimental data in Fig. 4a, which can be expressed by the non-linear form as follows:

$$k_2 = \frac{1}{t(c_a - c_b)} \ln \frac{c_b c_{at}}{c_a c_{bt}} \quad (1)$$

where c_a and c_b (mold m^{-3}) are the initial concentrations of phenylboronic acid and bromobenzene, c_{at} and c_{bt} (mold m^{-3}) are the concentrations of phenylboronic acid and bromobenzene when reaction time is t, respectively. The reaction rate constants (k_2, min^{-1}) of various catalysts are shown in Fig. 5, further demonstrating that $Pd_{0.10}/g\text{-}C_3N_4$ was the most efficient catalyst.

To optimize the reaction conditions, a series of experiments with different bases and solvents at different temperatures were conducted. As listed in Table 1, in the range of 25–55 °C, although the reaction rate increases with increasing the temperature, the satisfactory conversion (100%) can be obtained even at room temperature (25 °C) just for a slightly longer time of 40 min. Based on the principles of green chemistry, the Suzuki–Miyaura coupling reaction at room temperature should be an excellent choice.

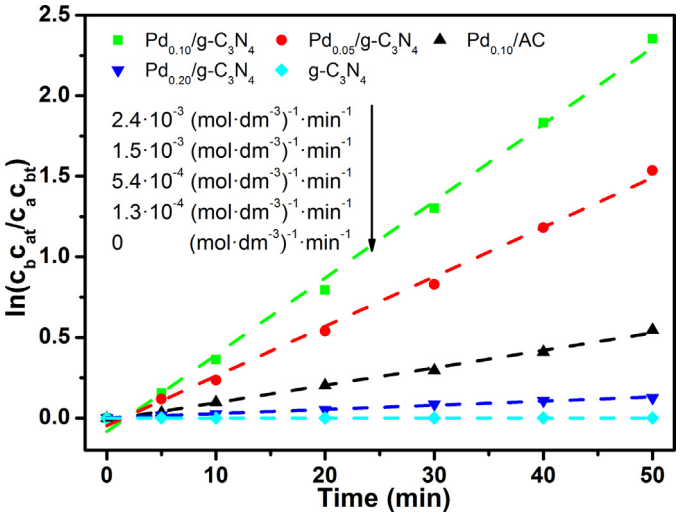

Fig. 5. Plot of $\ln(c_b c_{at}/c_a c_{bt})$ against reaction time for the Suzuki–Miyaura coupling reactions with various catalysts.

As known, bases can act as a bridge to connect bromobenzene and phenylboric acid, and the nature of base may influence the Suzuki–Miyaura coupling reaction. As shown in Table 2, KOH behaves as the most efficient base with 100% conversion of bromobenzene. Other inorganic bases such as K_2CO_3, $KHCO_3$, Na_2CO_3, $NaHCO_3$, NaOH and $NaOCH_3$ also gave the desired product in slightly less yields. Stronger inorganic bases seem to be more efficient in the reaction. In comparison, the results of organic bases weaker basicity, such as triethylamine (TEA), tributylamine (TBA) and 4-dimethylaminopyridine (DMAP), showed much poorer conversions.

The nature of solvent also is an important factor in the Suzuki–Miyaura coupling reaction. As can be seen in Table 3, the pure organic solvents like acetonitrile (ACN), tetrahydrofuran (THF), dimethylformamide (DMF), N-methylpyrrolidin-2-one (NMP), dimethylsulfoxide (DMSO), methanol (MeOH) and ethanol (EtOH) only exhibited lower conversions of 2–60% after

Table 1
Effect of temperature on the catalytic conversion.

Entry	Temperature (°C)	Conversion[a] (%)	Conversion[b] (%)
1	25	93.6	100.0
2	35	95.6	100.0
3	45	98.5	100.0
4	55	100.0	100.0

[a] Bromobenzene (0.2 mmol, 1 equiv), phenylboric acid (0.24 mmol, 1.2 equiv), KOH (0.6 mmol, 3 equiv), 4 mL H_2O:EtOH (1:1) and $Pd_{0.10}/g\text{-}C_3N_4$, 30 min.
[b] Bromobenzene (0.2 mmol, 1 equiv), phenylboric acid (0.24 mmol, 1.2 equiv), KOH (0.6 mmol, 3 equiv), 4 mL H_2O:EtOH (1:1) and $Pd_{0.10}/g\text{-}C_3N_4$, 40 min.

Table 2
Effect of bases on the catalytic conversion.[a]

Entry	Base	Conversion (%)
1	KOH	93.6
2	K_2CO_3	90.9
3	$KHCO_3$	82.5
4	NaOH	90.3
5	Na_2CO_3	87.1
6	$NaHCO_3$	78.6
7	$NaOCH_3$	65.4
8	TEA	9.3
9	TBA	30.2
10	DMAP	32.8

[a] Bromobenzene (0.2 mmol, 1 equiv), phenylboric acid (0.24 mmol, 1.2 equiv), 4 mL H_2O:EtOH (1:1) and $Pd_{0.10}/g\text{-}C_3N_4$, 25 °C, 30 min.

Table 3
Effect of solvents on the catalytic conversion.[a]

Entry	Solvent	Conversion (%)
1	ACN	2.7
2	THF	30.4
3	DMF	48.2
4	NMP	34.9
5	DMSO	39.4
6	MeOH	51.6
7	EtOH	59.3
8	DMF/H_2O (1:1)	76.1
9	DMSO/H_2O (1:1)	62.4
10	MeOH/H_2O (1:1)	85.2
11	EtOH/H_2O (1:1)	93.6

[a] Bromobenzene (0.2 mmol, 1 equiv), phenylboric acid (0.24 mmol, 1.2 equiv), KOH (0.6 mmol, 3 equiv), and $Pd_{0.10}$/g-C_3N_4, 25 °C, 30 min.

30 min. Instead, the addition of water to the organic solvents dramatically increased the reaction rates. This obvious improvement was on account of the fact that the poor solubility of the products in aqueous-ethanol solution would drive the equilibrium in favor of the product formation. Among the various water to ethanol ratios, the aqueous-ethanol (v/v = 1:1) solvent become the best medium for this catalytic system, exhibiting a high conversion of 93.6% within 30 min.

Under the optimized reaction conditions (in the presence of aqueous-ethanol (v/v = 1:1) solvent and KOH at room temperature), the catalytic performance of $Pd_{0.10}$/g-C_3N_4 was further examined for Suzuki–Miyaura coupling reaction of various aryl halides containing electron withdrawing or donating substituents (Table 4). The reaction of iodobenzene exhibited the complete conversion (100.0%) while that of chlorobenzene only showed a lower conversion of 38.6% within 30 min. The aryl bromides with either *m*-substituted or *p*-substituted —CHO all produced the corresponding biphenyl compounds with excellent yields (95.3%, 98.8%). However, the reaction of aryl bromides containing *o*-substituted —CHO gave slightly lower conversion (89.4%) due to the steric hindrance. More impressively, high catalytic activities were also found for aryl bromides with both electron-rich and electron-poor substituents, all affording the cross-coupling products in high yields.

Apart from the high catalytic activity, the $Pd_{0.10}$/g-C_3N_4 nanocomposite also displayed excellent cycle performance. As shown in Fig. 6a, $Pd_{0.10}$/g-C_3N_4 was applied to the coupling reaction of bromobenzene and phenylboric acid under the optimized reaction conditions. After the reaction, $Pd_{0.10}$/g-C_3N_4 catalyst was easily separated by a simple centrifugation technique and washed with NaOH solution and aqueous solution to remove the absorbed bromobenzene. The conversion rate of bromobenzene can maintain over 85% of the initial level after five cycles, exhibiting higher activity and higher stability than the commercial $Pd_{0.10}$/AC.

It is interesting to investigate whether the coupling reaction catalyzed by $Pd_{0.10}$/g-C_3N_4 or the leached homogeneous Pd species. First, $Pd_{0.10}$/g-C_3N_4 was dispersed in aqueous-ethanol (1:1) solvent with KOH via sonication, followed by filtration to remove the solid $Pd_{0.10}$/g-C_3N_4 catalyst. The corresponding amount of bromobenzene and phenylboronic acid was then added to the filtrate with magnetic stirring and no biphenyl was detected even after 1 h (Fig. 6b). The superior catalytic activity of Pd/g-C_3N_4 nanocomposite in Suzuki–Miyaura coupling reactions observed here can be attributed to the specific characteristics of the unique nanostructure of Pd/g-C_3N_4 and the concerted effects of g-C_3N_4 and Pd NPs. First of all, the porous g-C_3N_4 with graphitic planes constructed from tri-s-triazine units connected by planar amino groups has plenty of anchor sites for the Pd atoms, which is in favor to disperse and stabilize the Pd NPs. Secondly, g-C_3N_4 has analog structure with graphene (planar layers with π electron conjugation), the π–π stacking interaction between halobenzene molecules and

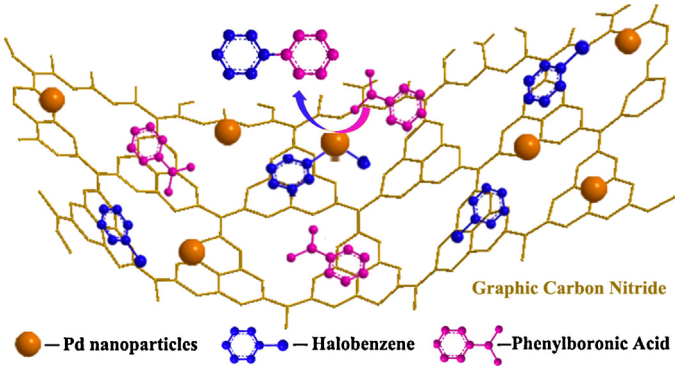

Scheme 2. Schematic diagram illustrating the mechanism of the Suzuki–Miyaura reaction catalyzed by Pd/g-C_3N_4 at room temperature.

g-C_3N_4 can help in promoting the reaction as the halobenzene molecules can easily gain access to Pd NPs. Accordingly, the mechanism of the Suzuki–Miyaura coupling reaction of halobenzene with phenylboronic acid catalyzed by Pd/g-C_3N_4 at room temperature is illustrated in Scheme 2: the absorbed halobenzene molecules can rapidly gain access to the well-dispersed Pd NPs on g-C_3N_4 via the oxidative addition and the resulting surface organopalladium species may connect with bases to fabricate an electrophilic

Table 4
Effect of aryl halides on the catalytic conversion.[a]

Entry	Aryl halide	Product	Conversion (%)
1		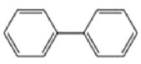	100.0
2	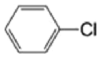	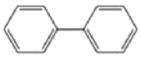	38.6
3	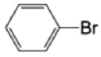	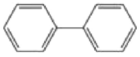	93.6
4	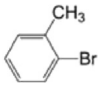	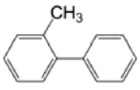	89.1
5	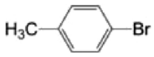	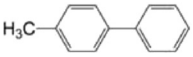	98.1
6	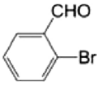	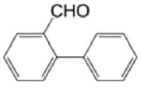	89.4
7		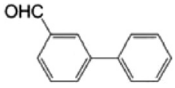	95.3
8	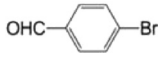	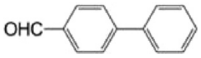	98.8
9	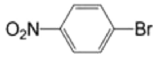	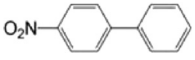	98.2
10	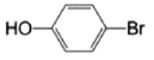	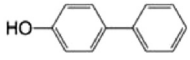	93.9
11	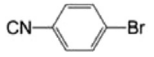	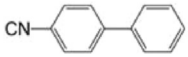	100.0
12	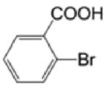	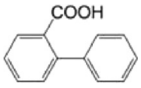	90.7

[a] Aryl halides (0.2 mmol, 1 equiv), phenylboric acid (0.24 mmol, 1.2 equiv), KOH (0.6 mmol, 3 equiv), 4 mL H_2O:EtOH (1:1) and $Pd_{0.10}$/g-C_3N_4, 25 °C, 30 min.

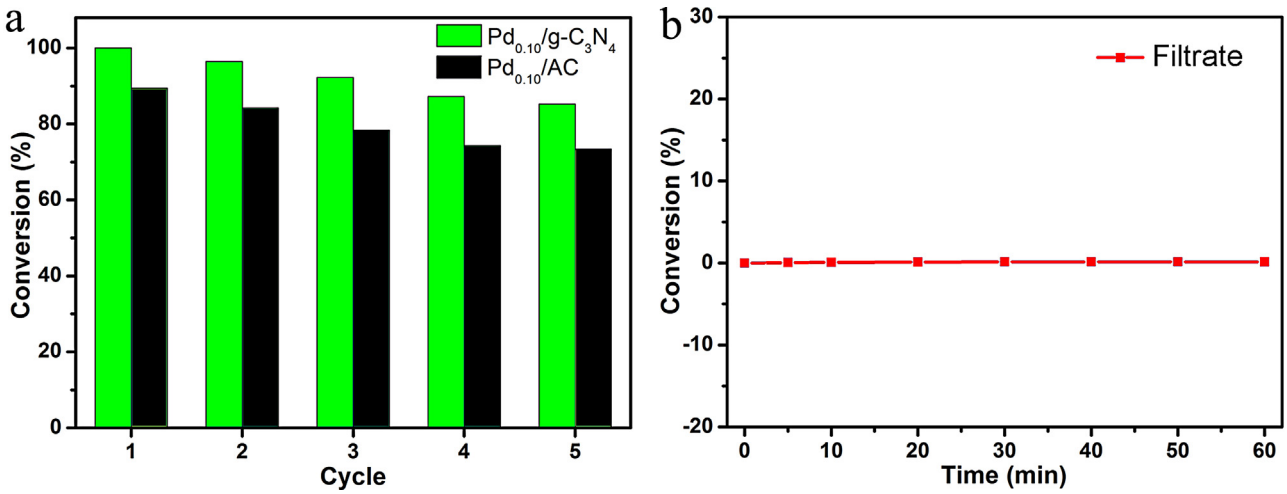

Fig. 6. (a) Reuse of $Pd_{0.10}/g\text{-}C_3N_4$ and $Pd_{0.10}$/AC catalysts for Suzuki–Miyaura coupling reaction, (b) Suzuki–Miyaura coupling reaction in the presence of the filtrate.

intermediate, which can be easily reacted with boron-ate complex through transmetalation, and consequently, the desired biphenyl is synthesized by means of reductive elimination, accompanying the restoration of the original catalyst.

4. Conclusion

In summary, a reusable $Pd/g\text{-}C_3N_4$ nanocomposite catalyst was designed and successfully prepared via a one-step photodeposition method. The catalyst exhibits high performance in Suzuki–Miyaura coupling reactions at room temperature without any phase transfer agents, toxic solvents and inert atmosphere, achieving green catalysis. The high catalytic activity of the catalyst can be attributed to the specific characteristics of the unique nanostructure of $Pd/g\text{-}C_3N_4$ and the concerted effects of $g\text{-}C_3N_4$ and ultrafine Pd particles, including that the porous $g\text{-}C_3N_4$ has plenty of nitrogen-containing anchor sites for the Pd atoms, which is in favor to disperse and stabilize the Pd nanoparticles, and the π–π stacking interaction between halobenzene molecules and $g\text{-}C_3N_4$ can help in promoting the reaction as the halobenzene molecules can easily gain access to Pd nanoparticles.

Acknowledgements

This work was supported by NNSF of China (No. 51322212) (No. 20123219130003), the Fundamental Research Funds for the Central Universities (Nos. 30920130122002, 30920140122003, 30920140122008), Jiangsu Planned Projects for Postdoctoral Research Funds (No. 1401003B), the Opening Project of the Jiangsu Key Laboratory for Environment Functional Materials (No. SJHG1303), the Jiangsu Province Key Laboratory of Fine Petrochemical Engineering (No. KF1206), the Zijin Intelligent Program of NUST (2014) and PAPD of Jiangsu.

References

[1] S.M. Raders, J.N. Moore, J.K. Parks, A.D. Miller, T.M. Leißing, S.P. Kelley, R.D. Rogers, K.H. Shaughnessy, J. Org. Chem. 78 (2013) 4649–4664.
[2] R. Martin, S.L. Buchwald, Acc. Chem. Res. 41 (2008) 1461–1473.
[3] Y.W. Zhao, H.L. Jin, H. Zhou, J.J. Lin, S. Wang, J.C. Wang, J. Phys. Chem. C 116 (2012) 7416–7420.
[4] N. Nicolaus, P.T. Franke, M. Lautens, Org. Lett. 13 (2011) 4236–4239.
[5] X.H. Li, M. Baar, S. Blechert, M. Antonietti, Sci. Rep. 3 (2013) 1743–1748.
[6] A. Fihri, M. Bouhrara, B. Nekoueishahraki, J.M. Basset, V. Polshettiwar, Chem. Soc. Rev. 40 (2011) 5181–5203.
[7] A. Molnaŕ, Chem. Rev. 111 (2011) 2251–2320.
[8] B.J. Borah, K. Saikia, P.P. Saikia, N.C. Barua, D.K. Dutta, Catal. Today 198 (2012) 174–183.
[9] C. Liu, Y.X. Zhang, N. Liu, J.S. Qiu, Green Chem. 14 (2012) 2999–3003.
[10] L. Xue, Z. Lin, Chem. Soc. Rev. 39 (2010) 1692–1705.
[11] K. Deplanche, J.A. Bennett, I.P. Mikheenko, J. Omajali, A.S. Wells, R.E. Meadows, J. Wood, L.E. Macaskie, Appl. Catal. B 147 (2014) 651–665.
[12] R.A. Reziq, H. Alper, D. Wang, M.L. Post, J. Am. Chem. Soc. 128 (2006) 5279–5282.
[13] M.R. Didgikar, D. Roy, S.P. Gupte, S.S. Joshi, R.V. Chaudhari, Ind. Eng. Chem. Res. 49 (2010) 1027–1032.
[14] G.B.B. Varadwaj, S. Rana, K. Parida, J. Phys. Chem. C 118 (2014) 1640–1651.
[15] M. Kim, J.C. Park, A. Kim, K.H. Park, H. Song, Langmuir 28 (2012) 6441–6447.
[16] A. Grirrane, A. Corma, H. Garciá, Science 322 (2008) 1661–1664.
[17] K.K.R. Datta, B.V.S. Reddy, K. Ariga, A. Vinu, Angew. Chem. Int. Ed. 49 (2010) 5961–5965.
[18] Y. Wan, H.Y. Wang, Q.F. Zhao, M. Klingstedt, O. Terasaki, D.Y. Zhao, J. Am. Chem. Soc. 131 (2009) 4541–4550.
[19] A. Modak, J. Mondal, A. Bhaumik, Green Chem. 14 (2012) 2840–2855.
[20] B.J. Gallon, R.W. Kojima, R.B. Kaner, P.L. Diaconescu, Angew. Chem. Int. Ed. 46 (2007) 7251–7254.
[21] R. Liu, M.M. Shannon, C. Li, R.U. Raymond, J.C. Idrobo, H.J. Gao, S.J. Pennycook, S. Dai, Angew. Chem. Int. Ed. 50 (2011) 6799–6802.
[22] G.M. Scheuermann, L. Rumi, P. Steurer, W. Bannwarth, R. Mulhaupt, J. Am. Chem. Soc. 131 (2009) 8262–8270.
[23] Y. Wang, J. Yao, H.R. Li, D.S. Su, M. Antonietti, J. Am. Chem. Soc. 133 (2011) 2362–2365.
[24] Y.Y. Bu, Z.Y. Chen, W.B. Li, Appl. Catal. B 144 (2014) 622–630.
[25] S. Obregón, G. Colón, Appl. Catal. B 144 (2014) 775–782.
[26] Y.T. Gong, P.F. Zhang, X. Xu, Y. Li, H.R. Li, Y. Wang, J. Catal. 297 (2013) 272–280.
[27] Y. Wang, X.C. Wang, M. Antonietti, Angew. Chem. Int. Ed. 51 (2012) 68–89.
[28] D.S. Deng, Y. Yang, Y.T. Gong, Y. Li, X. Xu, Y. Wang, Green Chem. 15 (2013) 2525–2531.
[29] E.Z. Lee, S.U. Lee, N.S. Heo, G.D. Stucky, Y.S. Jun, W.H. Hong, Chem. Commun. 48 (2012) 3942–3944.
[30] X.H. Li, X.C. Wang, M. Antonietti, Chem. Sci. 3 (2012) 2170–2174.
[31] H.J. Huang, X. Wang, Phys. Chem. Chem. Phys. 15 (2013) 10367–10375.
[32] J.W. Sun, Y.S. Fu, G.Y. He, X.Q. Sun, X. Wang, Catal. Sci. Technol. 4 (2014) 1742–1748.
[33] C. Chang, Y. Fu, M. Hu, C.Y. Wang, G.Q. Shan, L.Y. Zhu, Appl. Catal. B 142–143 (2013) 553–560.
[34] S.B. Yang, Y.J. Gong, J.S. Zhang, L. Zhan, L.L. Ma, Z.Y. Fang, R. Vajtai, X.C. Wang, P.M. Ajayan, Adv. Mater. 25 (2013) 2452–2456.
[35] D. Hollmann, M. Karnahl, S. Tschierlei, K. Kailasam, M. Schneider, J. Radnik, K. Grabow, U. Bentrup, H. Junge, M. Beller, S. Lochbrunner, A. Thomas, A. Brückner, Chem. Mater. 26 (2014) 1727–1733.
[36] X.C. Wang, K. Maeda, A. Thomas, K. Takanabe, G. Xin, J.M. Carlsson, K. Domen, M. Antonietti, Nat. Mater. 8 (2009) 76–80.
[37] J.S. Zhang, X.F. Chen, K. Takanabe, K. Maeda, K. Domen, J.D. Epping, X.Z. Fu, M. Antonietti, X.C. Wang, Angew. Chem. Int. Ed. 49 (2010) 441–444.
[38] H. Xu, J. Yan, Y.G. Xu, Y.H. Song, H.M. Li, J.X. Xia, C.J. Huang, H.L. Wan, Appl. Catal. B 129 (2013) 182–193.
[39] Y.G. Li, J.A. Zhang, Q.S. Wang, Y.X. Jin, D.H. Huang, Q.L. Cui, G.T. Zou, J. Phys. Chem. B 114 (2010) 9429–9434.
[40] B.V. Lotsch, M. Doblinger, J. Sehnert, L. Seyfarth, J. Senker, O. Oeckler, W. Schnick, Chem. Eur. J. 13 (2007) 4969–4980.